EUROPEAN ORGANIZATION FOR NUCLEAR RESEARCH

CERN-EP/86-03
10 January 1986

TOTAL, ELASTIC, AND INCLUSIVE SINGLE-DIFFRACTIVE CROSS-SECTIONS IN ALPHA-ALPHA COLLISIONS AT THE CERN INTERSECTING STORAGE RINGS +)

D. Lloyd Owen[1)]
CERN, Geneva, Switzerland

G. Paternoster and S. Patricelli
Dipartimento di Fisica dell'Università and INFN, Naples, Italy

V. Cavasinni, T. Del Prete, M. Morganti and F. Schiavo
Dipartimento di Fisica dell'Università and INFN, Pisa, Italy

G. Anzivino[2)]
State University of New York, Stony Brook, NY, USA

ABSTRACT

We present measurements of the total interaction cross-section and of the single-diffractive dissociation cross-section in $\alpha\alpha$ collisions at $\sqrt{s}$ = 126 GeV. The result obtained for the total cross-section, σ_{tot} = (315 ± 18) mb, is a substantial improvement on the precision of earlier measurements. Earlier elastic data were re-analysed, incorporating, through the optical theorem, the present σ_{tot} measurement, resulting in improved determinations of the forward slope, $b_{-t<0.07}$ = (87 ± 4) GeV^{-2}, and of the integrated elastic cross-section, σ_{el} = (58 ± 6) mb. The single-diffractive differential cross-section falls exponentially with momentum transfer at small values of t with a slope b_{sd} = (19.3 ± 0.6) GeV^{-2}. The integrated single-diffractive cross-section is σ_{sd} = (16.7 ± 2.5) mb. The topology of charged tracks resulting from the disintegration of the α in single-diffractive events reveals a two-component distribution. The cross-section data are compared with multiple-scattering models.

(Submitted to Nuclear Physics B)

+) This article is dedicated to the memory of our friend and colleague Giorgio Alberi.
1) Present affiliation: Centre d'Études Nucléaires de Saclay, Gif-sur-Yvette, France.
2) Present affiliation: CERN, Geneva, Switzerland.

1. INTRODUCTION

The interest in studying collisions of nuclei, rather than those of single hadrons, is that more of the underlying dynamics of the strong interactions is potentially revealed in such collisions. The mean free path of hadrons in nuclear matter is of the order of or smaller than nuclear diameters, so that multiple interactions can occur separated by space–time intervals comparable with the space–time range of the strong interactions, leading to interference effects that are absent in the collisions of single hadrons.

Whether or not it is possible to isolate those aspects of the dynamics revealed in this way depends on the complexity of the projectiles, and therein lies the specific interest in $\alpha\alpha$ interactions and in the comparison of $\alpha\alpha$ and pp collisions: the α is the simplest compact nucleus (the deuteron is relatively weakly bound) and the average number of nucleonic interactions per $\alpha\alpha$ collision is only about two.

In the context of the measurements accessible to our experiment, the situation regarding 'inelastic intermediate states' (IIS) is of particular interest. It has been suggested that, at sufficiently high energies, the standard Glauber multiple-scattering expansion has to be generalized to allow for the diffractive excitation of a massive state in one constituent collision followed by its return to the ground state in the subsequent collision. The status of IIS is experimentally an open question: two experiments [1, 2] appeared to have found evidence supporting the IIS hypothesis, whereas later experiments disputed this [3, 4]. As we show later, our total and elastic cross-section results tend to favour the IIS hypothesis.

In addition to the total and elastic cross-sections, the study of inclusive single diffraction can improve our understanding of light-nuclei interactions. Also, in this case, the Glauber model has to be modified to account for the experimental results. Our measurement of the single-diffraction scattering is in agreement with previous experiments [1, 2] and confirms the existence of unusual interference phenomena.

The first studies of high-energy $\alpha\alpha$ interactions were conducted by a number of experiments in two runs at the CERN Intersecting Storage Rings (ISR) in mid-1980, and, despite the brevity of these runs, a surprising amount of physics emerged from them*). At the time of these first runs, our experimental apparatus was only partially installed, consisting then of the small-angle elastic telescopes (TB) and the luminosity-monitor hodoscopes (H_{34}). Nevertheless, this was sufficient to measure [6] the differential elastic cross-section in a momentum-transfer range that extended into the forward peak, and to estimate the total hadronic cross-section both for $\alpha\alpha$ interactions at c.m.s. energy $\sqrt{s} = 126$ GeV and for αp interactions at $\sqrt{s} = 89$ GeV.

The present communication presents results obtained from the 126 GeV $\alpha\alpha$ data taken with the complete R210 detector during the second period of light-ion runs at the ISR in August 1983. The detector is briefly described in section 2; section 3 deals with the measurement of the total cross-section, and with the impact that this measurement has on our earlier elastic results; section 4 discusses the study of single-diffractive scattering; in section 5 we compare the cross-section results with some model calculations, and finally, in section 6, we summarize all results.

2. EXPERIMENTAL APPARATUS

The apparatus (described in detail elsewhere [7]) was designed to measure total and elastic cross-sections in pp and $p\bar{p}$ interactions. It consisted of scintillation-counter hodoscopes spanning the entire azimuth in the polar region $0.2° < \theta < 179.8°$. Each of the two identical arms of the detector (surrounding the exiting beam pipes) contained five hodoscopes — CIO, H_{12},

*) A comprehensive review of both the physics and the technical aspects of these and the later light-ion runs at the ISR has been given by Faessler [5].

H_{34}, H_5, and TB—which overlapped in θ. The coverage of these hodoscopes in pseudorapidity ($\eta = -\ln \tan \theta/2$) was: $0.0 < |\eta| < 1.5$ (CIO); $1.2 < |\eta| < 3.0$ (H_{12}); $2.5 < |\eta| < 4.5$ (H_{34}); $4.0 < |\eta| < 5.0$ (H_5); and $4.5 < |\eta| < 6.0$ (TB). Each 'H' hodoscope consisted of two planes of trigger counters, operated in coincidence, and a third plane of annular counters to localize charged secondaries in θ and ϕ.

The TB telescopes were located symmetrically at 9.2 m from the intersection point. Each telescope consisted of the following:

- Two planes of scintillation counters (TB_A and TB_B), which provided the α trigger. The pulse height of individual counters was also recorded to provide specific-ionization measurements.
- Two arrays of 9 'finger' scintillators (TB_y), each 25 mm × 90 mm. The arrays consisted of two planes staggered horizontally by 12.5 mm.
- Two arrays of drift tubes (DT) [8], each array consisting of two planes of 12 tubes staggered vertically to resolve up/down ambiguities. The tube was a cylinder, 10 mm in diameter and 300 mm in length, with 250 μm aluminium walls and a 40 μm sense wire along the cylindrical axis.

The basic trigger of the data acquisition was a coincidence between hits in the left and the right arm:

$$\begin{aligned} \mathrm{Hit}_{L,R} &= (\mathrm{CIO} \oplus H_{12} \oplus H_{34} \oplus H_5 \oplus \mathrm{TB})_{L,R} \\ \mathrm{Trigger} &= \mathrm{Hit}_L \otimes \mathrm{Hit}_R \,. \end{aligned} \tag{1}$$

Specific-ionization measurements in the TB trigger counters formed the basis of an α-particle identification off-line. Time-of-flight (TOF) measurements between left- and right-hand trigger hodoscopes were used to reject single-beam background, also off-line.

The data were collected during the August 1983 light-ion runs at the ISR. The α currents were typically about 5 A, giving a luminosity $L \approx 0.8 \times 10^{29}$ cm^{-2} s^{-1}, as monitored by the $H_{34L} \otimes H_{34R}$ coincidence rate. Luminosity-monitor calibrations were performed using the Van der Meer (VdM) method [9].

3. TOTAL CROSS-SECTION ANALYSIS

The $\alpha\alpha$ total cross-section was measured using the total-rate method: $\sigma_{tot} = R_{tot}/L$, where R_{tot} is the total hadronic interaction rate of the colliding α beams and L is their luminosity. The total rate R_{tot} was greater than the trigger rate R_{obs} because of losses due to the incomplete solid-angle coverage of the detector. The dead regions—the holes in the TB hodoscopes accommodating the vacuum chamber—resulted in a loss of forward events having low single-arm multiplicity: primarily elastic events but also events with a single-diffractive topology. The total cross-section was, therefore, measured in three parts:

$$\begin{aligned} \sigma_{tot} &= \sigma_{obs} + \Delta\sigma_{el} + \Delta\sigma_{inel} \,, \\ \sigma_{obs} &= R_{obs}/L \,. \end{aligned} \tag{2}$$

The observed cross-section, which constituted about 75% of the total cross-section, was measured during the luminosity-calibration runs. The high quality of beam control, typical of ISR operations, meant that these runs were virtually free of the principal source of background, i.e. single-beam interactions. Figure 1, which shows the VDM calibration curve of the trigger, is an indication of the cleanliness of these runs. After background subtraction, the experimental curve was integrated with respect to beam separation in the standard manner to yield the observed cross-section:

$$\sigma_{obs} = (243 \pm 12)\,\mathrm{mb} \,, \tag{3}$$

where the error is predominantly systematic, representing the 5% uncertainty in the calibration of the beam-displacement scale. This result is in good agreement with the 'production' cross-section, $\sigma_{prod} = (265 \pm 26)$ mb, reported by the CERN–Heidelberg–Lund Collaboration [10] (R418), whose definition of σ_{prod} corresponded closely to our definition of σ_{obs}.

The $\Delta\sigma$ correction to σ_{obs} was calculated by extrapolating measured angular distributions into the dead regions and performing over those regions Monte Carlo (MC) integrations that took account of detector geometry, of the finite extent of the beam-overlap zone, and of the shape of the extrapolated distribution.

In the case of the inelastic losses two forms—both of a single-diffractive character—were investigated. In the first case, the event topology studied required an identified α at small angles in one arm and anything (other than an elastically scattered α) in the second arm. The details of this single-diffractive analysis are discussed in the following section. In the second case, the α-identification criterion was dropped in order to study the angular dependence of 'quasi-diffractive' events, i.e. those events in which the object recoiling against the diffractively scattered system was not an α but a collimated, low-multiplicity cluster arising from the fragmentation of an α. Apart from the pulse-height requirement, the event selection and the analysis of the quasi-diffractive sample were the same as those of the single-diffractive sample.

The inelastic losses computed by the MC on the basis of the angular slopes extracted by the two analyses were

$$\Delta\sigma_{inel} = \Delta\sigma_{sd} + \Delta\sigma_{qd}$$

with

$$\Delta\sigma_{sd} = (13.0 \pm 0.1)\,\text{mb} \tag{4}$$

and

$$\Delta\sigma_{qd} = (1.0 \pm 0.1)\,\text{mb}\,.$$

The differential cross-section for $\alpha\alpha$ elastic scattering at $\sqrt{s} = 126$ GeV has been measured in different t ranges by three ISR experiments: our own experiment [6] ($0.05 < -t < 0.8$ GeV^2); the R418 [11] experiment ($0.2 < -t < 0.8$ GeV^2); and R807 the Axial Field Spectrometer experiment [12] ($0.05 < -t < 0.19$ GeV^2). The cross-section was found to be a very rapidly falling exponential in the small-t region ($-t < 0.07$ GeV^2). This small-angle peak is followed by a minimum at $-t \approx 0.1$ GeV^2 and a secondary maximum at $-t \approx 0.4$ GeV^2, beyond which the t dependence is again roughly exponential.

In the elastic-loss MC, the differential cross-section was parametrized as an exponential (slope b_1) at small angles ($-t < -t_1$), as flat in the region of the dip and second maximum ($-t_1 < -t < -t_2$), and as a second exponential (slope b_2) at larger angles ($-t > -t_2$). Normalization of the cross-section was accomplished via the optical theorem (assuming that ϱ, the real-to-imaginary ratio of the forward elastic amplitude, was zero). The correction term calculated by the MC was sensitive to the value used for b_1, but relatively insensitive to the values of the other parameters.

Our earlier measurement of the small-t slope gave a value $b_1 = (100 \pm 10)$ GeV^{-2}. Experiment R807, with superior t resolution, found $b_1 = (72 \pm 6)$ GeV^{-2}. Both measurements were hampered by the strength of the t dependence and the restricted t range accessible within the peak.

The total and forward elastic cross-sections are, however, coupled through the optical theorem, and this extra constraint permitted the iterative calculation of both the total cross-section and the forward slope. The values of the slopes, the correction term, the integrated elastic cross-section, and the total cross-section, at convergence were:

$$
\begin{aligned}
b_1 &= (87 \pm 4)\ \mathrm{GeV}^{-2}\ ; \\
\sigma_{el} &= (58 \pm 6)\ \mathrm{mb}\ ; \\
\Delta\sigma_{el} &= (58 \pm 6)\ \mathrm{mb}\ ; \\
\sigma_{tot} &= (315 \pm 18)\ \mathrm{mb}\ .
\end{aligned}
\tag{5}
$$

(Statistical and systematic errors have been combined.) The elastic loss amounted to 98% of the total elastic cross-section, only (0.4 ± 0.1) mb being detected.

These results represent a considerable improvement in precision over previous measurements. Our earlier best estimate, derived from the $H_{34L} \otimes H_{34R}$ inclusive cross-section, was $\sigma_{tot} = (295 \pm 40)$ mb; while R807, extrapolating their elastic measurement to the optical point, found $\sigma_{tot} = (280 \pm 70)$ mb. The only other measurements of $\sigma_{tot}^{\alpha\alpha}$ were made at the Berkeley Bevalac at $\sqrt{s} \approx 9$ and 11 GeV. The values found [13], i.e. $\sigma_{tot} = (408 \pm 2.5)$ and (390 ± 4.2) mb, respectively, suggest that the cross-section depends weakly on s and is decreasing.

Having measured both total and elastic cross-section, we can estimate the values of the 'geometrical-scaling' ratios σ_{el}/σ_{tot} and b_1/σ_{tot}. In the context of geometrical scaling, the quantities σ_{tot}, σ_{el} and $b = d \ln (d\sigma_{el}/dt)/dt|_{t=0}$ are all proportional to the mean square radius of the interaction $\langle R^2 \rangle$, which is simply related to b. From our results:

$$
\begin{aligned}
\sigma_{el}/\sigma_{tot} &= 0.184 \pm 0.004\ , \\
b_1/\sigma_{tot} &= 0.276 \pm 0.020\ , \\
\sqrt{\langle R^2 \rangle} &= (2.60 \pm 0.06)\ \mathrm{fm}\ .
\end{aligned}
\tag{6}
$$

It is striking that these ratios are consistent, within errors, with those measured [14] in pp and $p\bar{p}$ interactions at $\sqrt{s} = 53$ GeV: the pp ratios are 0.176 ± 0.004 and 0.310 ± 0.009, respectively. The r.m.s. interaction radius derived for pp at $\sqrt{s} = 63$ GeV is $\sqrt{\langle R^2 \rangle} = (1.02 \pm 0.02)$ fm.

4. DIFFRACTIVE CROSS-SECTION ANALYSIS

The diffractive analysis was based on data collected with the same fully inclusive trigger as that used for the total cross-section analysis [eq. (1)]. Candidate single-diffractive events ($\alpha\alpha \rightarrow \alpha X$) were extracted from this sample off-line by imposing a topological requirement equivalent to the trigger:

$$
\begin{aligned}
\mathrm{Trigger}_{sd} = {} & TB_L \otimes \overline{(H_5 \oplus H_{34} \oplus H_{12})}_L \otimes (CIO \oplus H_{12} \oplus H_{34} \oplus H_5)_R \\
& \oplus (H_5 \oplus H_{34} \oplus H_{12} \oplus CIO)_L \otimes \overline{(H_{12} \oplus H_{34} \oplus H_5)}_R \otimes TB_R\ .
\end{aligned}
\tag{7}
$$

The veto requirement ensured a rapidity gap of ≥ 4.5 units between the α and the next largest angle track in the α arm (isolation cut). Spurious vetoes, due to event pile-up, were negligible (< 1%). The absence of a TB component in the opposite arm was a minimum angle requirement of $\theta \geqslant 0.6°$ on the X cluster, and thus excluded elastic events. These requirements removed most of the inelastic background from the initial sample, which was reduced from 800,000 to 16,000 events.

The sample was then further refined by imposing a pulse-height cut on the TB counters detecting the α candidate. This cut removed almost all of the residual background, leaving a sample of 8,000 events, with an estimated background contamination of < 5%.

The efficiency of the selection criteria was investigated in some detail by varying the isolation cut and observing the effect on the resultant TB pulse-height spectrum. We estimate the efficiency to be about 90%, independent of the α angle, but we performed no correction for this relatively small inefficiency.

The production of δ-rays in the TB telescope gave rise to spurious tracks accompanying the α-tracks in 19% of the events. While this did not affect the efficiency of the trigger, it did lead to

ambiguities in the determination of the trajectory of the α. Such events were excluded from the calculation of the differential cross-section. To achieve the correct scale we multiplied the cross-section so obtained by a factor of 1.24, assigning an estimated scale error of $\pm 5\%$ for the uncertainty in this procedure.

The angular resolution was limited by the finite dimensions of the beam-crossing region. Angular cells were thus defined by the overlap of drift-tube and scintillation-counter cells (5 mm by 12.5 mm), which gave an angular resolution comparable to the limit set by the extent of the source. The mean polar angle and the acceptance of all cells was computed by a MC which took account of the shape of the ultimate cross-section and of finite source size, as well as of detector geometry. Polar angles were transformed into momentum transfers assuming that the scattered α's retained the full beam momentum: $t = 2p_{ISR}^2(\cos\theta - 1)$. The resolution in t was $\pm 0.02\ \mathrm{GeV}^2$.

The single diffractive cross-section is shown in fig. 2 and listed in table 1. In both cases, the errors are statistical and do not include a 15% systematic error, which arises from uncertainties in the luminosity, in the geometry, and in the correction factor for the δ-ray veto. The t dependence of the cross-section is roughly exponential in the t range explored, and the solid line in the figure is a fit*) to the data in the region $-t < 0.2\ \mathrm{GeV}^2$

$$d\sigma_{sd}/dt = (160 \pm 7)e^{(19.3 \pm 0.6)t}\ \mathrm{mb/GeV^2}\,; \quad \chi^2/\mathrm{d.f.} = 83/40\,. \tag{8}$$

The data in the region $-t > 0.2\ \mathrm{GeV}^2$ are consistently higher than the fit, indicating the persistence at this energy of the structure observed not only in low-energy $\alpha\alpha$ diffractive scattering [15] but also in αp [2] and dd [16] interactions.

This departure is in disagreement with Glauber model predictions incorporating non-peripheral nucleon profile functions that successfully account for elastic scattering. The larger t behaviour can, however, be reproduced by adding a peripheral component to the profile function and, at the same time, by including non-negligible contributions from helicity-flip amplitudes. Peripherality in coherent diffraction dissociation causes a peculiar constructive interference between single- and multiple-scattering amplitudes and it is this that accounts for the observed structure at larger t in αp and dd as well as in $\alpha\alpha$ interactions [15].

Integrating our measured $d\sigma_{sd}/dt$ over the full t range, we obtained:

$$\sigma_{sd} = (16.6 \pm 2.5)\ \mathrm{mb}\,, \tag{9}$$

where statistical and systematic errors have been combined.

The system X that recoils against the α was analysed in terms of its multiplicity and angular properties using the fine-grained planes of the hodoscopes. No attempt was made to correct for the instrumental effects (finite counter size, photon conversions, secondary interactions, etc.) to which the detector was subject; instead we rely on a comparison of distributions, rather than the distributions themselves to form a qualitative understanding of the physics.

The mean pseudorapidity of charged tracks $\bar{\eta}$ and the dispersion D_η in η were calculated for each event. The polarity of η was defined — event by event — such that the α was at $\eta > 0$, but the α itself was excluded from the calculation. The distribution of events in these two quantities is shown in the scatter plot in fig. 3a. For comparison, fig. 3b shows the same distribution but for minimum-bias (MB) events with the requirement of at least one track in a TB hodoscope, this track then defining positive polarity in η**). Whereas the minimum-bias sample (which, though

---

*) It was this fit that was used to calculate the σ_{tot} correction terms $\Delta\sigma_{sd}$.

**) The MB plots correspond to an integrated luminosity of about a factor of 10 smaller than the corresponding SD ones, in order to prevent blurring of the physical picture due to a too large number of plotted points.

dominated by 'multiperipheral' events, contained an admixture of single-diffractive events) is characterized by a small $\bar{\eta}$ and large D_η ($\langle\bar{\eta}\rangle \approx 0$, $\langle D_\eta\rangle \approx 2.4$), the single-diffractive sample has, as expected, an asymmetrical distribution with smaller dispersion ($\langle\bar{\eta}\rangle \approx 2.8$), $\langle D_\eta\rangle \approx 1.0$). Figure 3a, however, reveals that there are two components to the $\bar{\eta}$–D_η distribution: one with larger $\langle\bar{\eta}\rangle$ and smaller $\langle D_\eta\rangle$ than the other.

Let us call the large $\langle\bar{\eta}\rangle$/small $\langle D_\eta\rangle$ component the 'quasi-elastic' (QE) component, since it populates the boundaries of phase space*); in contradistinction, we shall now restrict the term 'single-diffractive' (SD) to the other component.

The separation of the two components is enhanced when $\bar{\eta}$–D_η distributions are plotted semi-inclusively, i.e. in different ranges of charged multiplicity n. Figures 4–6 are the semi-inclusive analogues of fig. 3 for $n \leq 5$, $5 < n \leq 10$, and $n > 10$, respectively. In the low-multiplicity diffractive plot (fig. 4a) QE events predominate, whereas in the high-multiplicity plot (fig. 6a) their presence is markedly attenuated. The obvious interpretation is that the SD events arise from interactions in which a relatively high-mass object is formed, the dispersion in η of its decay products reflecting the parent mass distribution. In QE interactions, on the other hand, the diffracted cluster, with large η and smaller spread in η, results from an α which is excited to a mass not much above the ground state, and which subsequently breaks up with no, or very few, particles being created.

The differential cross-section $d\sigma_{qe}/dt$ was computed, exploiting the separation of SD and QE events in $\bar{\eta}$–D_η space, and is plotted in fig. 7 and listed in table 2 (statistical errors only). The cross-section is again an exponential in t (broken line in fig. 7), and was fitted with

$$d\sigma_{qe}/dt = (31 \pm 5)\, e^{(25 \pm 2)t}\ \text{mb/GeV}^2\,, \quad \chi^2/\text{d.f.} = 60/29\,. \tag{10}$$

(The continuous line in the figure represents the elastic cross-section scaled down by an order of magnitude.) The slope of the QE cross-section is significantly steeper than that of the SD cross-section, but still nowhere near as steep as the elastic one. Integrating over t, we found

$$\sigma_{qe} = (1.2 \pm 0.2)\text{mb}\,. \tag{11}$$

The mean $\bar{n}$ and the dispersion D_n of the multiplicity of the SD, QE, and MB events in fig. 3 were calculated, and are presented in table 3. The SD and QE values are broadly similar, both being smaller than for the MB sample.

5. COMPARISON WITH MODELS

Early ISR investigations [1] of hadron–nucleus and nucleus–nucleus elastic scattering indicated a deficiency in the traditional Glauber multiple-scattering approach [17] that could be remedied by incorporating inelastic intermediate states (IIS), or inelastic screening, into the model. This was confirmed by a FNAL experiment [2], but more recent data [3, 4], as previously mentioned, differ from the ISR experiment, at least in respect to the size of the effect. Alberi and co-workers [19] calculated the various contributions to the $\alpha\alpha$ total cross-section at $\sqrt{s} = 126$ GeV, including (excluding) IIS, and found $\sigma_{tot} = 289$ (386) mb, a value differing by -10 $(+20)\%$ from our measurement. The non-diffractive inelastic part of the cross-section, which roughly corresponds to σ_{obs} [eq. (3)], was calculated to be 180 (225) mb, or -25 $(-7)\%$

*) We investigated the possibility that the QE events might, in reality, be true elastic events in which the α suffered a secondary interaction in ambient material. The computed probability for such an effect is far smaller than the effect itself, and the measured angular distribution of the unperturbed α is inconsistent with the elastic differential cross-section. We, therefore, rejected such a possibility.

different from the measurement. The two approaches differed most radically in their estimation of the elastic cross-section, giving σ_{el} = 61 (113) mb—the IIS calculation being clearly favoured by our data.

Relevant cross-section calculations have also been performed in the framework of an additive quark model (AQM) [20] and reproduce almost exactly the pure-Glauber results for σ_{tot} and σ_{el}. The calculation of the non-diffractive and diffractive inelastic contributions to the total cross-section ($\sigma_{nd} \approx 230$ mb; $\sigma_d \approx 20$ mb), however, are in good agreement with the data. In their calculations, the authors of ref. [20] used an approximation that neglected excited states of the colliding objects. Were the effect of incorporating such states into AQM to be comparable to that of IIS in the Glauber model, the result would be in excellent agreement with the data.

6. CONCLUSIONS

We measured the total $\alpha\alpha$ cross-section via the total-rate method, achieving higher precision than in previous experiments. The σ_{tot} determination permitted a re-evaluation of earlier elastic data, resulting in improved estimates of the forward slope and of the integral of the differential elastic cross-section. A separate analysis isolated single-diffractive events and determined the angular dependence and integral of the differential cross-section for such interactions. Total, elastic, and single-diffractive cross-section results are summarized in table 4.

The topology of the diffractively excited system resulting from a single-diffractive scattering reveals two separate components: in the majority of cases, the cluster recoiling from the α has relatively high mass; in about 7% of cases, the cluster has a mass not much higher than the α mass.

A comparison of the cross-section results with current multiple-scattering models reveals some discrepancies. On the whole, however, the results support the hypothesis of intermediate inelastic states. An extension of the additive quark model to include excitations of the collision participants might well bring it into good agreement with the data.

Acknowledgements

The advice and assistance of G. Carboni, P.D. Grannis and M. Valdata-Nappi are greatly appreciated. The technical assistance of G.C. Barnini, A. Bechini, L. Giacomelli and T. Regan is gratefully acknowledged. We wish to thank the staff of the Linac, of the Proton Synchrotron and, especially, of the Intersecting Storage Rings Division, whose unfailing skill and dedication made this experiment possible.

REFERENCES

[1] G. Goggi et al., Phys. Lett. **77B** (1978) 428 and 433;
G. Goggi et al., Nucl. Phys. **B149** (1979) 381.

[2] A. Bujak et al., Phys. Rev. **D23** (1981) 1895.

[3] J.P. Burq et al., Nucl. Phys. **B187** (1981) 205.

[4] G. Warren et al., Nucl. Phys. **B207** (1982) 365.

[5] M. Faessler, Phys. Rep. **115** (1984) 1.

[6] M. Ambrosio et al., Phys. Lett. **113B** (1982) 347.

[7] G. Carboni et al., Nucl. Phys. **B254** (1985) 697.

[8] U. Becker et al., Nucl. Instrum. Methods **180** (1981) 61.

[9] S. Van der Meer, CERN Internal Report ISR-PO/68-31 (1968).

[10] W. Bell et al., Phys. Lett. **128B** (1983) 349.

[11] W. Bell et al., Phys. Lett. **117B** (1982) 131.

[12] T. Åkesson et al., Phys. Lett. **152B** (1985) 140.

[13] J. Jaros et al., Phys. Rev. **C18** (1978) 2273.

[14] M. Ambrosio et al., Phys. Lett. **115B** (1982) 495.

[15] J. Duflo et al., Nucl. Phys. **A356** (1981) 427;
T. Fujita and J. Hüfner, Phys. Lett. **87B** (1979) 327.

[16] G. Goggi et al., Lett. Nuovo Cimento **24** (1979) 381;
G. Goggi et al., Nucl. Phys. **B161** (1979) 14;
G. Goggi and G. Alberi, Lett. Nuovo Cimento **27** (1980) 229.

[17] R.J. Glauber, *in* Lectures in Theoretical Physics, Vol. 1 (eds. W.C. Brittin and L.G. Durham) (Interscience, New York, 1959).

[18] G. Alberi and G. Goggi, Phys. Rep. **74** (1981) 1.

[19] G. Alberi, A. Malecki and V. Roberto, Lett. Nuovo Cimento **36** (1983) 409.

[20] A. Białas, W. Czyż and L. Leśniak, Z. Phys. **C13** (1982) 147.

[21] N. Amos et al., Nucl. Phys. **B262** (1985) 689.

Table 1

Differential single-diffractive cross-section

$\|t\|$ (GeV^2)	$d\sigma/dt$ (mb/GeV^2)	$\|t\|$ (GeV^2)	$d\sigma/dt$ (mb/GeV^2)
0.044	57.7 ± 4.4	0.200	5.8 ± 0.8
0.051	59.4 ± 3.2	0.210	2.7 ± 0.5
0.060	51.5 ± 4.2	0.233	5.0 ± 0.6
0.067	45.2 ± 2.7	0.236	3.0 ± 0.5
0.073	47.6 ± 2.9	0.241	2.3 ± 0.6
0.078	37.8 ± 3.6	0.262	2.4 ± 0.5
0.085	32.0 ± 2.4	0.268	2.0 ± 0.5
0.089	33.9 ± 2.4	0.275	1.9 ± 0.6
0.098	17.9 ± 2.5	0.289	2.6 ± 0.7
0.105	18.1 ± 1.8	0.300	1.2 ± 0.3
0.107	27.9 ± 2.4	0.312	2.5 ± 0.7
0.120	10.4 ± 1.9	0.319	1.2 ± 0.5
0.127	14.0 ± 1.1	0.350	0.3 ± 0.2
0.145	6.9 ± 1.5	0.400	0.3 ± 0.1
0.151	7.9 ± 0.8	0.450	0.3 ± 0.1
0.175	6.1 ± 0.8	0.600	0.10 ± 0.06
0.183	5.0 ± 0.6	0.850	0.0 ± 0.06

Table 2

α-differential cross-section in quasi-elastic events

$\|t\|$ (GeV^2)	$d\sigma/dt$ (mb/GeV^2)	$\|t\|$ (GeV^2)	$d\sigma/dt$ (mb/GeV^2)
0.044	11.0 ± 1.9	0.127	0.86 ± 0.2
0.051	7.0 ± 1.1	0.144	1.1 ± 0.3
0.060	6.9 ± 1.6	0.150	0.6 ± 0.2
0.067	8.6 ± 1.2	0.163	1.2 ± 0.4
0.073	8.5 ± 1.2	0.173	0.3 ± 0.3
0.077	2.9 ± 1.1	0.183	0.2 ± 0.2
0.085	4.4 ± 0.7	0.201	0.5 ± 0.3
0.089	5.4 ± 1.0	0.21	0.3 ± 0.2
0.098	3.1 ± 1.1	0.230	0.0 ± 0.2
0.106	2.1 ± 0.4	0.265	0.2 ± 0.2
0.110	4.4 ± 0.7		

Table 3

Comparative multiplicity distributions for single-diffractive (SD), quasi-elastic (QE) and minimum-bias (MB) events in $\alpha\alpha$ interactions (raw multiplicities)

	$\langle\bar{\eta}\rangle$	$\langle D_\eta \rangle$	$\langle n \rangle$	D_n
SD	-2.85 ± 0.05	1.05 ± 0.02	5.59 ± 0.08	3.69
QE	-4.40 ± 0.05	0.32 ± 0.02	4.43 ± 0.13	3.16
MB	0.00 ± 0.01	2.45 ± 0.01	24.5 ± 0.1	12.7

Table 4

Final results of total cross-section analysis.
Results obtained in pp and $\bar{p}p$ interactions are also reported.

$\sqrt{s} = 126$ GeV		$\sqrt{s} = 53$ GeV			
$\alpha\alpha$		pp	[Ref.]	$\bar{p}p$	[Ref.]
σ_{tot} (mb)	315 ± 18	43.01 ± 0.27	[7]	44.71 ± 0.46	[7]
		42.38 ± 0.15	[21]	43.32 ± 0.34	[21]
σ_{sd} (mb)	16.6 ± 0.5	8.5 ± 2.5	[18]	-	
σ_{qe} (mb)	1.2 ± 0.2	-		-	
σ_{el} (mb)	58 ± 6	7.8 ± 0.2	[14]	7.9 ± 0.2	[14]
		7.17 ± 0.09	[21]	7.44 ± 0.32	[21]
b_1 (GeV^{-2})	87 ± 4	13.1 ± 0.4	[14]	13.9 ± 0.4	[14]
		12.87 ± 0.14	[21]	13.03 ± 0.52	[21]
σ_{el}/σ_{tot}	0.185 ± 0.004	0.180 ± 0.003	[14]	0.176 ± 0.004	[14]
		0.169 ± 0.002	[21]	0.172 ± 0.007	[21]
b_1/σ_{tot} (GeV^{-2} mb^{-1})	0.28 ± 0.02	0.302 ± 0.009	[14]	0.310 ± 0.009	[14]

Figure captions

Fig. 1 The VDM calibration curve for the trigger [eq. (1)].

Fig. 2 The single-diffractive differential cross-section. The curve is the fit of eq. (8). (The errors shown are statistical only.)

Fig. 3 Scatter plot of $\bar{\eta}$ versus D_η (a) for the single-diffractive sample; and (b) for the minimum-bias sample. (See text.)

Fig. 4 Scatter plot of $\bar{\eta}$ versus D_η (a) for single-diffractive events with $n \leq 5$; and (b) for minimum-bias events with $n \leq 5$. (See text.)

Fig. 5 Scatter plot of $\bar{\eta}$ versus D_η (a) for single-diffractive events with $5 < n < 10$; and (b) for minimum-bias events with $5 < n < 10$. (See text.)

Fig. 6 Scatter plot of $\bar{\eta}$ versus D_η (a) for single-diffractive events with $n > 10$; and (b) for minimum-bias events with $n > 10$. (See text.)

Fig. 7 The quasi-elastic differential cross-section. The broken curve is the fit of eq. (10). (The errors shown are statistical only.) The solid line is the elastic differential cross-section scaled down by a factor of 10.

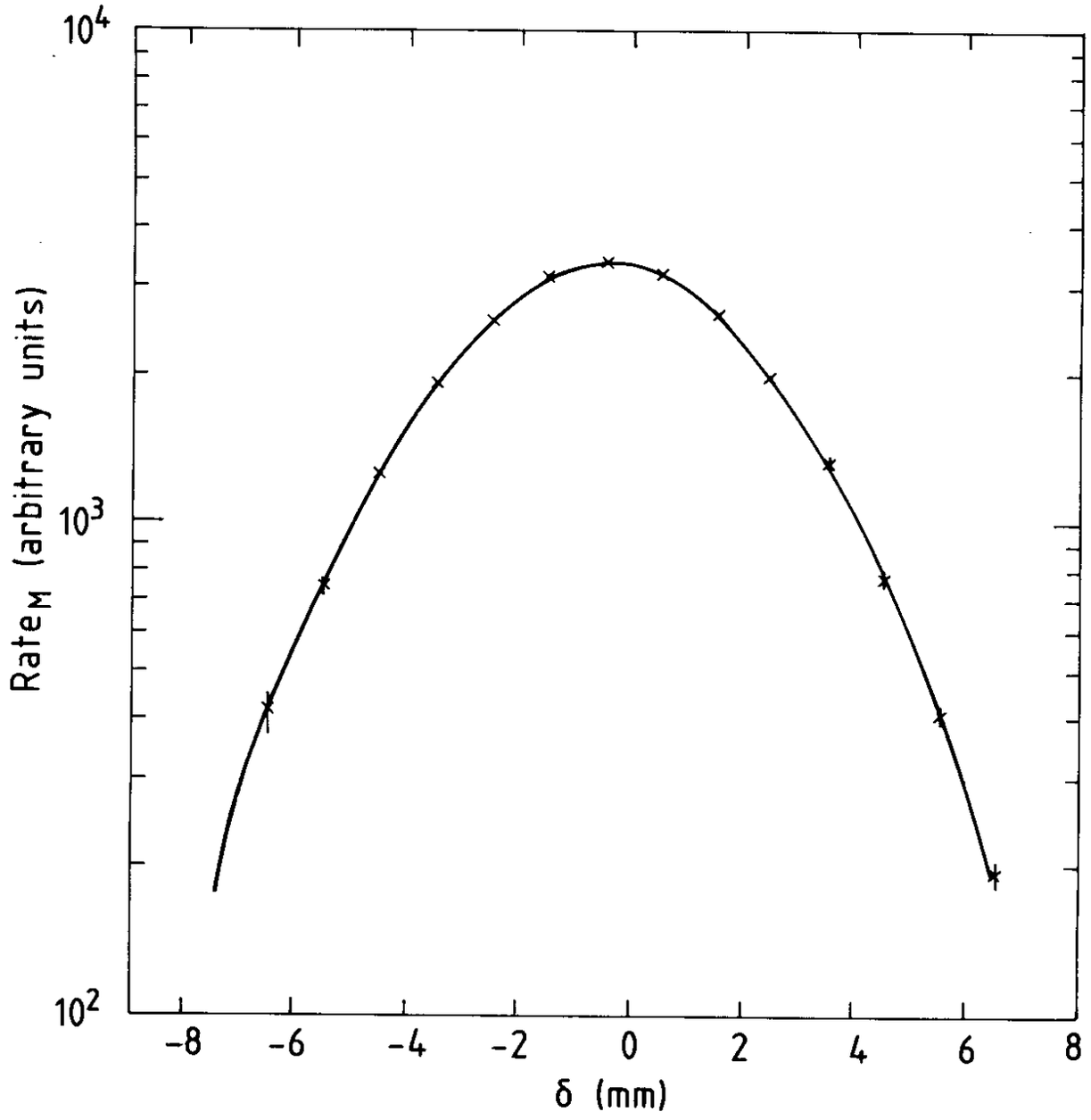

Fig. 1

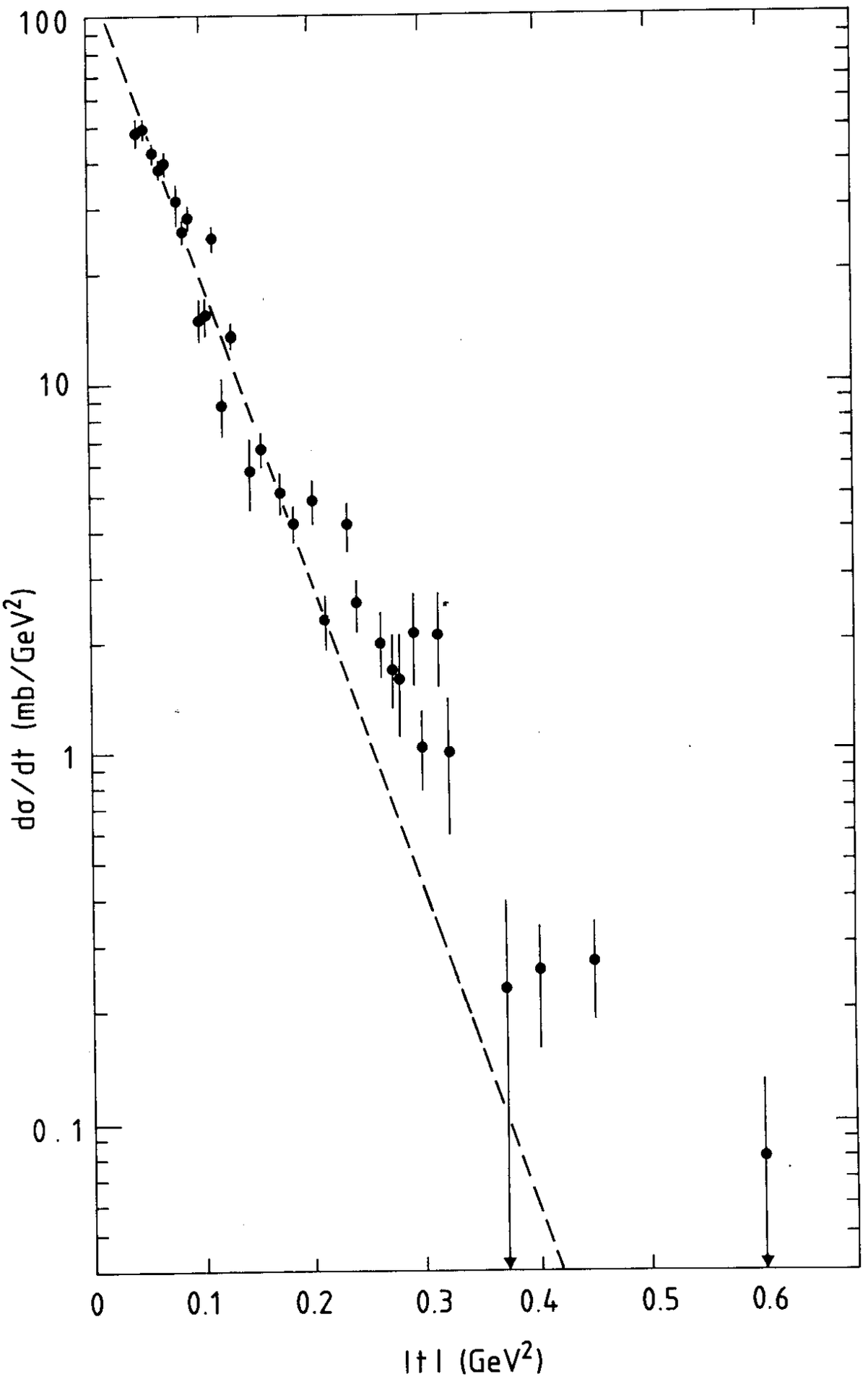

Fig. 2

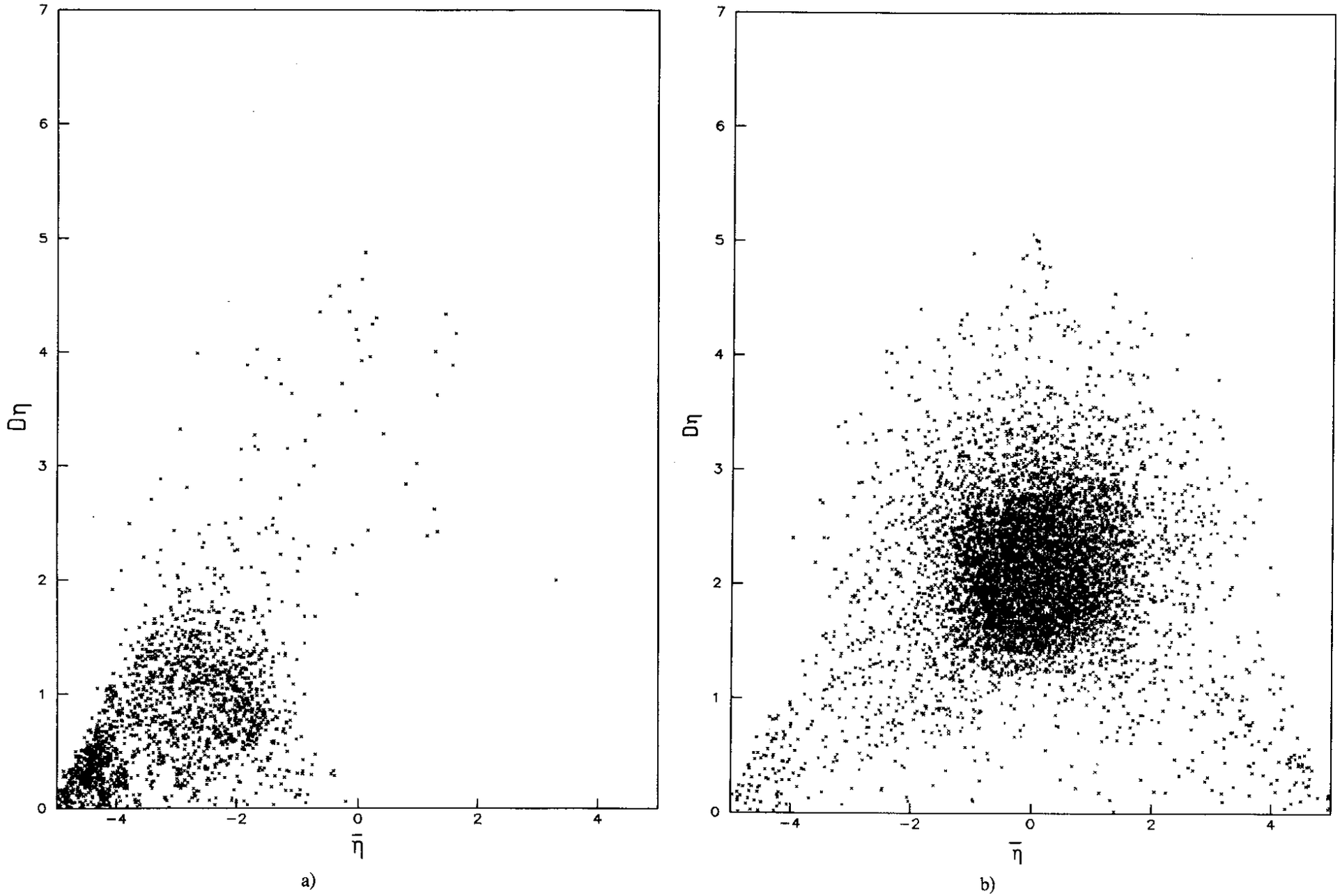

Fig. 3

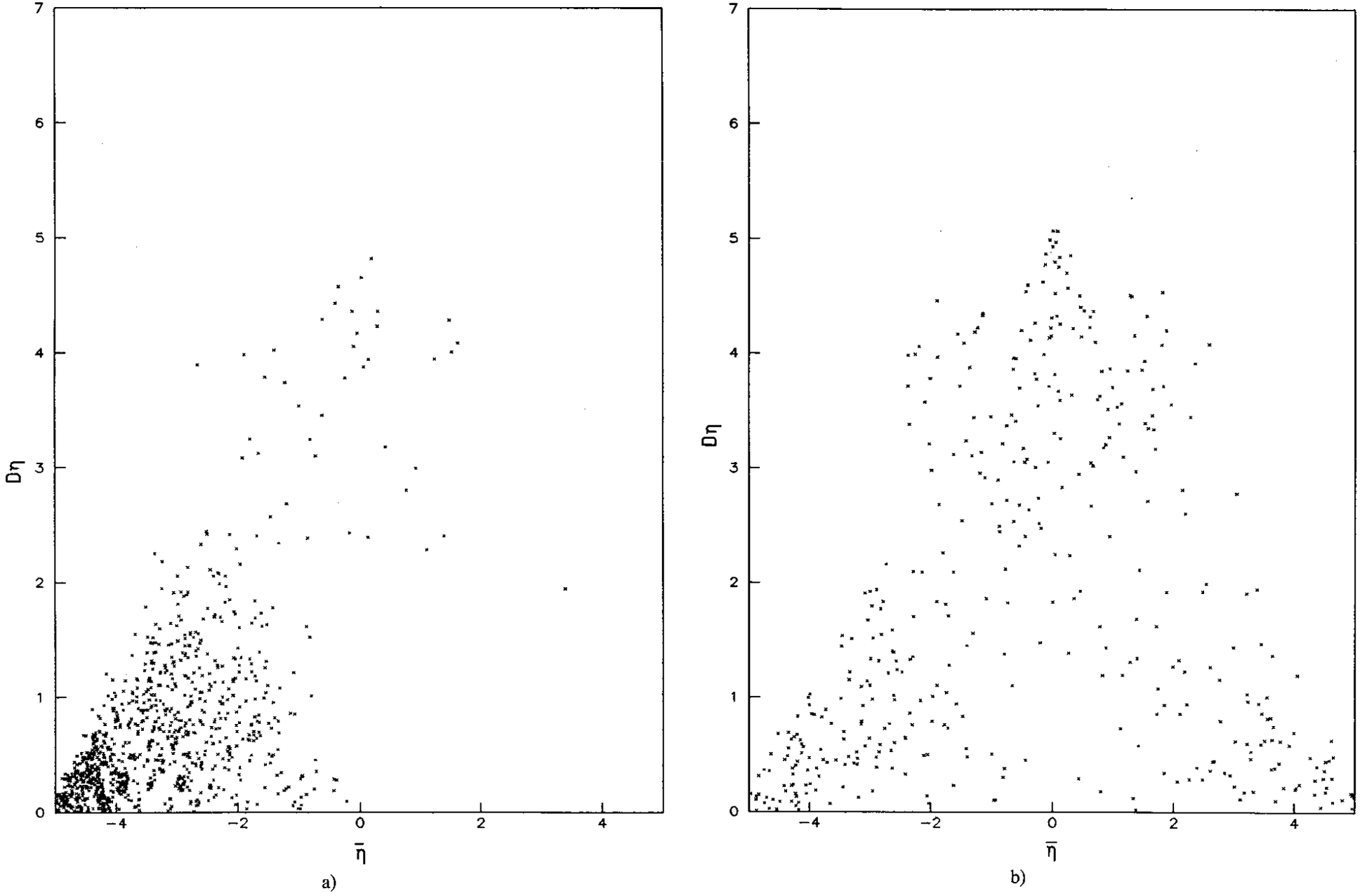

Fig. 4

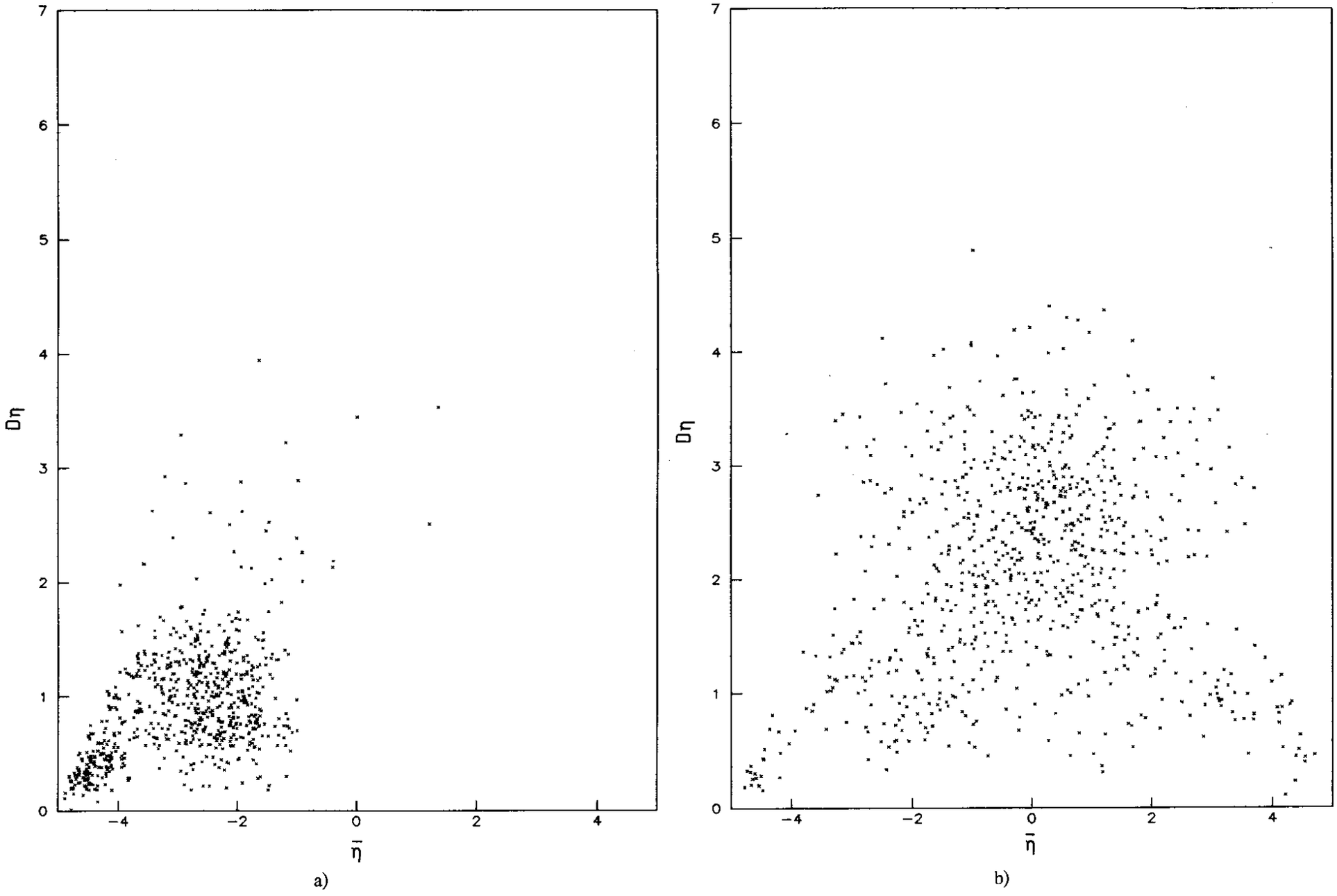

Fig. 5

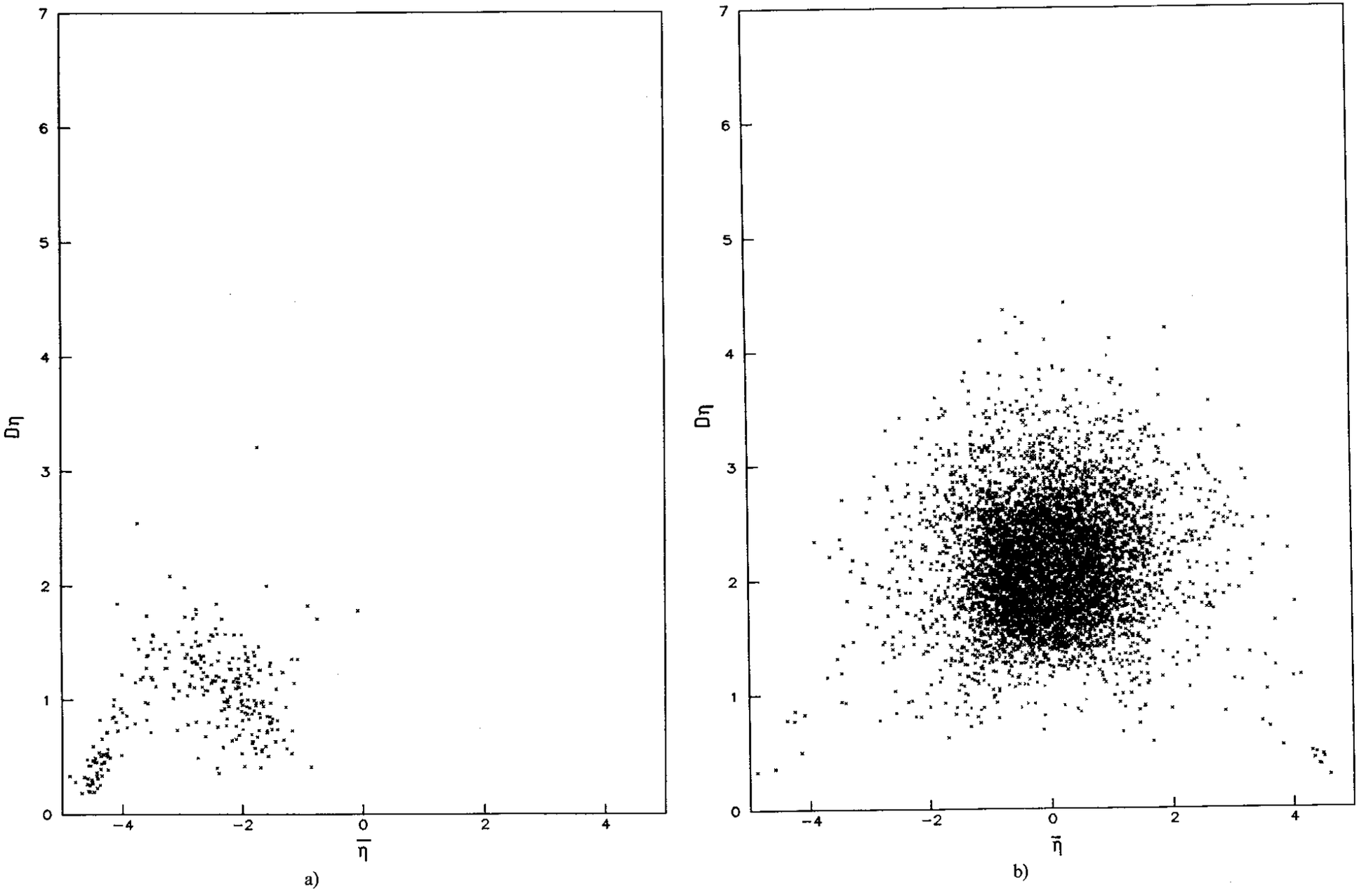

Fig. 6

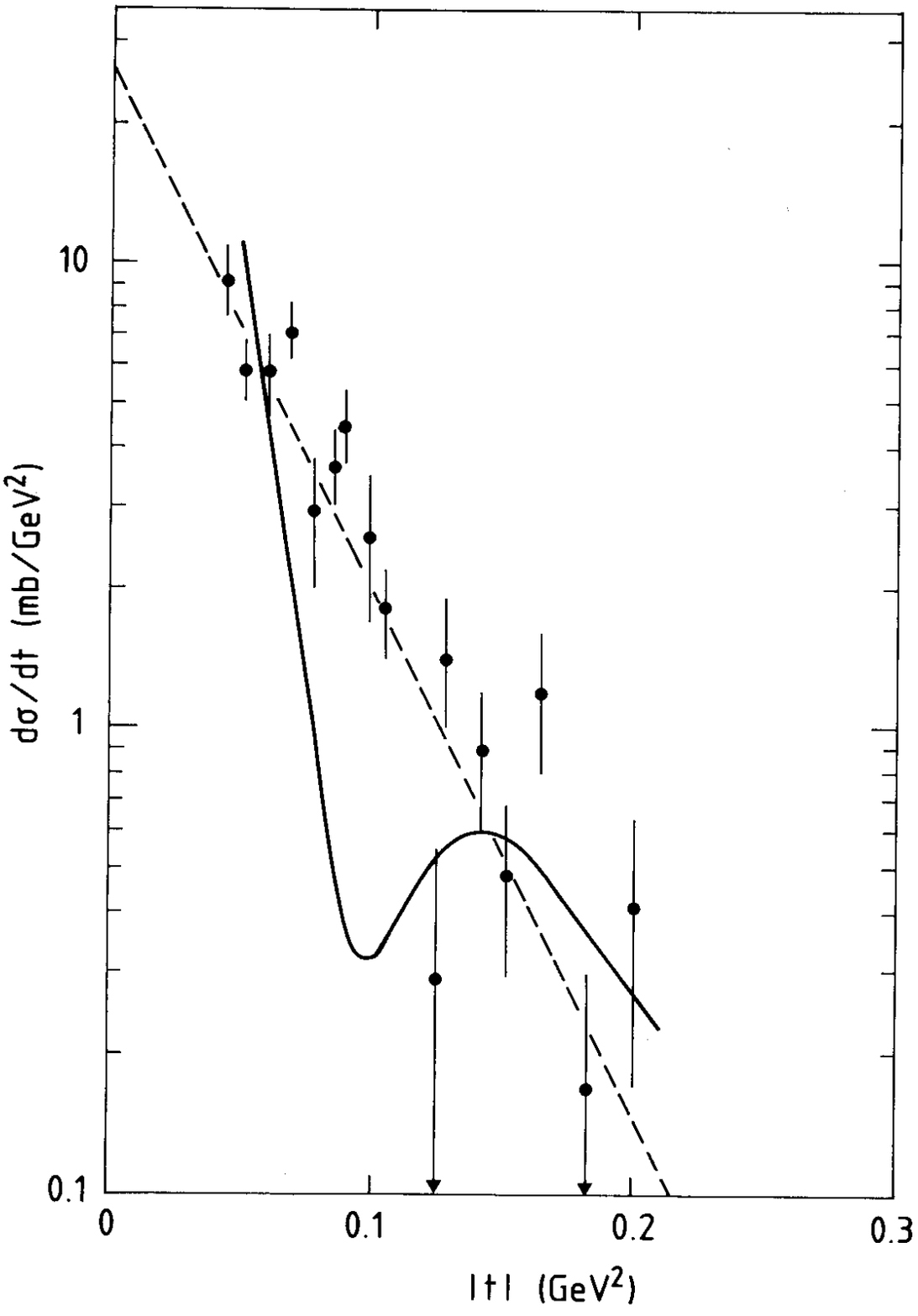

Fig. 7